Materials Today Electronics 11 (2025) 100140

Contents lists available at ScienceDirect

Materials Today Electronics

journal homepage: www.elsevier.com/locate/mtelec

Review

Graphene metasurfaces: Advances in lens applications, design strategies, and fabrication techniques

Meisam Esfandiari, Xiaojing Lv, Shaghayegh Chamani, Yang Yang *

School of Electrical and Data Engineering, University of Technology Sydney (UTS), Sydney, NSW, Australia

ARTICLE INFO

Keywords:
Lens
Graphene
Metasurfaces
Tunability

ABSTRACT

This review comprehensively examines the recent advancements in graphene-based metasurface lenses, shedding light on their innovative design principles, advanced manufacturing techniques, and superior optical properties. Graphene's exceptional electrical, mechanical, and optical characteristics, combined with the versatile functionality of metamaterials and metasurfaces, have led to the development of highly efficient and dynamic lens systems. These lenses demonstrate remarkable capabilities, including tunable focal lengths, enhanced light modulation, and improved photodetection sensitivity. Such properties render them highly suitable for transformative applications in diverse fields like high-resolution imaging, precision sensing, and next-generation telecommunications. The review provides an in-depth analysis of the state-of-the-art methods used in the fabrication of these lenses, such as chemical vapor deposition, advanced lithography, and nanomanufacturing, to achieve nanoscale precision and functional integration. Moreover, the challenges associated with large-scale production scalability, fabrication techniques' complexity, and graphene's long-term stability under varying environmental conditions are critically examined. In exploring these aspects, the review identifies key directions for future research, emphasizing the need for interdisciplinary collaboration to overcome current limitations. By addressing these challenges and leveraging advancements in material science and nanotechnology, graphene-based metasurface lenses have the potential to revolutionize the future of optical lens systems and photonic technologies.

1. Introduction

1.1. Graphene

Graphene is a remarkable material composed entirely of carbon atoms arranged in a hexagonal lattice [1–4]. Carbon atoms in graphene possess six electrons; two occupy the inner shell, while the remaining four fill the outer shell. Three of these four electrons create robust covalent bonds with neighbouring atoms, conferring strength to the graphene sheet. The fourth outer-shell electron is delocalized, moving freely across the graphene layer and enabling electrical conductivity [5–8]. Pristine graphene differs from typical insulating or semiconducting materials because it lacks a bandgap between the valence and conduction bands [9]. This zero-gap property renders graphene a unique material, functioning as both a zero-gap semiconductor and, at times, a metallic material when the Fermi level is positioned at the intersection point of the conduction and valence (Dirac point) [10–12].

Graphene's versatility in switching between semiconductor and metallic states makes it highly valuable for photonic applications requiring transparency and conductivity in ultra-thin films. The position of the Fermi level can be tuned, adjusting the balance between graphene's semiconductor and metallic properties. This adjustment can be achieved through chemical modifications or an electric field. For instance, when a biasing is applied between a graphene sheet and an underlying metal base, separated by a thin insulating layer, the electric field alters the number of charge carriers and, consequently, the electrical conductivity of graphene. A positive voltage polarity increases the electron concentration in the conduction band, while a negative polarity fills the conduction band states with electrons, creating holes in the system [13–15].

1.2. Surface conductivity of graphene

It is important to understand that the graphene sheet's frequency-dependent surface conductivity (σ) for both the surface conductivity and the thin film models, which can be obtained using microscopic or

* Corresponding author.
E-mail address: yang.yang-1@uts.edu.au (Y. Yang).

https://doi.org/10.1016/j.mtelec.2025.100140
Received 28 December 2024; Received in revised form 6 February 2025; Accepted 20 February 2025
Available online 21 February 2025

experimental measurements. Here, the Kubo Model is used to derive the following high-frequency expression [16–18]:

$$\sigma(\mathrm{w}) = \frac{\mathrm{e}^2(w + i\gamma_c)}{\mathrm{i}\pi\hbar^2}\left[\int_{-\infty}^{+\infty}\frac{|\epsilon|}{(w+i\gamma_c)^2}\frac{\mathrm{d}f_0(\epsilon)}{\mathrm{d}\epsilon}\mathrm{d}\epsilon - \int_0^{+\infty}\frac{f_0(-\epsilon)-f_0(\epsilon)}{(w+i\gamma_c)^2-4\left(\frac{\epsilon}{\hbar}\right)^2}\mathrm{d}\epsilon\right]. \tag{1}$$

In the formula, e is the electron charge, $\hbar$ (h/2π) is the reduced Planck constant and γ_c is a phenomenological carrier scattering rate. The fermi function is: $f_0(\epsilon) = \left\{\exp\left[\frac{\epsilon-\mu_c}{K_B\,T}\right] + 1\right\}^{-1}$, that μ_c and K_B are the chemical potential and Boltzmann's constant, respectively, and T is the ambient temperature.

Eq. (1) includes two terms: the first represents the Intraband electron-photon scattering transition, and the second characterizes the Interband electron transition. For graphene, which is free from chemical additives and zero gate voltage, at T = 0 K, charge carrier concentration (n_0) is very low. However, this value can be adjusted by changing chemical potential doping or applying a DC voltage. The following conditions define the chemical potential:

$$n_0 = \frac{2}{\pi\hbar^2 v_F^2}\int_0^{+\infty}\epsilon\left[f_0(\epsilon) - f_0(\epsilon + 2\mu_c)\right]\mathrm{d}\epsilon, \tag{2}$$

where $v_F \approx 9.5 \cdot 105\ \mathrm{MS}^{-1}$ is the Fermi velocity.

1.2.1. Intraband conductivity

The Intraband term in Eq. (1) leads to [19–21]:

$$\sigma^{\mathrm{intra}}(\mathrm{w}) = \frac{2ie^2K_BT}{\pi\hbar^2(w+i\gamma_c)}\ln\left[2\cosh\left(\frac{\mu_c}{2k_BT}\right)\right]. \tag{3}$$

If $\mu_c \gg K_BT$, the carriers exhibit degeneracy, causing the material to behave like a metal. In this scenario, $n_0 \approx \pi\hbar^2 v_F^2$, and the chemical potential can be stated as $\mu_c \approx E_F \approx \sqrt{\pi\hbar^2 v_F^2}$, where E_F is the Fermi energy, and finally, the intraband term can be estimated as:

$$\sigma^{\mathrm{intra}}(\mathrm{w}) = \frac{ie^2|\mu_c|}{\pi\hbar^2(w+i\gamma_c)}. \tag{4}$$

The real part of the intraband conductivity, denoted as $\mathrm{Re}(\sigma_{\mathrm{intra}})$, is non-negative, while the imaginary part, $\mathrm{Im}(\sigma_{\mathrm{intra}})$, is positive. *Re* and Im represent a complex quantity's real and imaginary components. Since σ_{intra} relates to surface impedance Z, a positive $\mathrm{Im}(\sigma_{\mathrm{intra}})$ results in Im (Z)<0, indicating an inductive surface impedance. This property is crucial, as the imaginary part of surface impedance fundamentally influences the boundary's ability to guide surface waves. The imaginary part's sign of the surface impedance is essential in metallic surfaces, as it determines that transverse electric (TE) or transverse magnetic (TM), can propagate along the boundary.

1.2.2. Interband conductivity

The Interband of conductivity contribution comprises real and imaginary components. Under low-temperature conditions, this contribution can be closely approximated when $|\mu_c|$ significantly exceeds k_BT (with μ_c as the chemical potential and K_BT as thermal energy) [22–24]:

$$\sigma^{\mathrm{inter}}(\mathrm{w}) = \frac{e^2}{4\hbar^1}\left[\theta(\hbar^1 w - 2|\mu_c|) + \frac{i}{\pi}\ln\left|\frac{\hbar^1(w+i\gamma_c)-2|\mu_c|}{\hbar^1(w+i\gamma_c)+2|\mu_c|}\right|\right]. \tag{5}$$

The probability of such electrons jumping from the valence band to the conduction band in graphene at low temperatures without high-energy photons (such as visible or ultraviolet) is quite low. This results in a near absence of interband transitions. Consequently, under standard conditions, especially at lower temperatures and in the absence of external optical excitation, the interband conductivity of graphene approaches zero, attributable to the scarcity of available states for these transitions within the low-energy spectrum. Besides that, graphene's electronic properties imply that at the Dirac point (the position of the Fermi level in undoped graphene), no density of states will support the conduction, hence further reducing the probability of interband transitions [25].

1.3. Graphene permittivity

The surface conductivity of graphene is primarily influenced by intraband transitions, as previously discussed. Notably, graphene functions as a conductive layer that can be accurately described by the Drude model, allowing it to support TM-polarized surface plasmon polaritons (SPPs). The surface conductivity of graphene exhibits a linear dependence on the Fermi level (E_F). In the terahertz frequency range, intraband transitions dominate, leading to significant losses; however, these losses are beneficial for amplitude modulation through graphene absorption. Conversely, the conductivity decreases at mid-infrared frequencies due to Pauli blocking and the relatively higher frequency, which reduces intraband and interband transitions. In this frequency range, the imaginary part of the conductivity becomes more prominent than the real part, facilitating the propagation of TM SPPs with minimal losses. For numerical simulations, graphene is often modelled as an anisotropic medium with an effective in-plane permittivity. This representation highlights the unique interaction between graphene and electromagnetic waves across different frequencies, emphasizing its tunability and effectiveness in supporting TM SPPs as [26–28]:

$$\epsilon_{\mathrm{eff,t}} = 1 + \frac{i\sigma_g}{\epsilon_0 w t_g}, \tag{6}$$

where ϵ_0 is the vacuum permittivity, t_g is the thickness of graphene.

Graphene's conductivity can be broadly adjusted at terahertz and mid-infrared frequencies, allowing substantial changes in plasmon resonance amplitude or frequency when it is critically coupled with a metasurface that enhances local fields. This tunability enables graphene to respond dynamically to electromagnetic fields, enhancing its application in amplitude and frequency modulation. Additionally, as an ultrathin "metal" layer, graphene can be patterned into various shapes to achieve targeted resonance frequencies and specific wavefront modifications. Such customization makes graphene highly versatile in advanced photonic and plasmonic applications, enabling precise control over light-matter interactions and supporting the design of structures for tailored optical responses.

2. Graphene-based metasurface

Metasurfaces consist of subwavelength structures that are typically much smaller than the wavelength of incoming electromagnetic waves [29,30]. These constructs can be ingeniously designed to impart specific properties to the impinging electromagnetic waves, such as phase modulation, polarization conversion, and focusing [31]. However, the key bottleneck associated with metasurfaces is their passive nature, implying that the optical properties become fixed during the time of fabrication itself [32].

Hence, hybrid graphene/metasurfaces or graphene-based metasurfaces will emerge due to their synergistic properties in a larger range of adaptable and powerful applications, such as antennas [33] and biosensors [34,35].

In the frequency range of microwaves, effective impedance matching can be challenging in devices incorporating graphene, and thus, it will affect operational efficiency regarding devices like antennas and transistors. Within the terahertz frequency spectrum, the intraband transitions contribute to most surface conductivity in graphene. The imaginary part of permittivity outperforms its real counterpart, demonstrating the high impact of intrinsic losses due to intraband transitions on graphene's optical properties. The Fermi-level controlled

huge variation of surface conductivity in graphene enables amplitude modulation with large magnitude when combined with metallic metasurfaces that support efficient confinement of in-plane electric fields [36,37]. The transmission change originates primarily from the variation of graphene absorbance:

$$\Delta T = -\Delta A \sim S|E_{inc}|^2 \eta^2 \Delta Re(\sigma_s). \quad (7)$$

In this context, S represents the graphene area, E_{inc} denotes the incident electric field, and $\eta = E/E_{inc}$ signifies the enhancement factor [38,39]. As indicated in Eq. (7), a considerable modulation depth can be achieved with a markedly improved field despite the surface conductivity being of comparatively low quality. Additionally, by adjusting graphene, metallic resonators can produce highly amplified local fields for terahertz modulation and sensing [40–43]. For example, SRRs are electric resonances, the sandwich structures are magnetic resonances, and asymmetric configurations are Fano resonances [44,45]. Additionally, the optical properties developed in graphene/plasmonic metasurface mainly involve changes in resonant frequency that are supposed to be tuned by varying the Fermi level of the graphene [46–48].

2.1. Graphene/Dielectric metasurfaces

The previous discussion emphasized the potential of hybrid graphene/metallic metasurfaces in various applications. However, one significant limitation of metallic metasurfaces is their susceptibility to non-radiative losses, particularly in the near-infrared (NIR) and optical frequency ranges. These losses result in resonances characterized by low Q-factors and a constrained modulation depth, limiting their effectiveness in high-performance photonic systems [49–52].

Dielectric metasurfaces have garnered considerable attention to address these drawbacks. According to Mie's theory, dielectric metasurfaces, typically composed of high-refractive-index particles embedded within a low-refractive-index medium, offer distinct advantages. They can support both electric and magnetic resonances while maintaining inherently low intrinsic losses. This unique combination of properties has led to their consideration as promising alternatives to metallic metasurfaces in many photonic and optoelectronic applications.

However, despite these advantages, the practical realization of dielectric metasurfaces introduces several challenges. Fabrication demands extraordinarily high machining precision to achieve the required dimensions and tolerances, as the optical response is highly sensitive to structural parameters. Furthermore, achieving optimal transmission properties necessitates a substantially elevated Fermi level, which exceeds the capabilities of traditional electrostatic gating techniques. This limitation poses significant hurdles to integrating these metasurfaces into dynamically tunable devices [53,54].

Another critical challenge is the lack of experimental demonstrations showcasing dynamic tunability in graphene/dielectric metasurfaces. While theoretical frameworks and computational models suggest promising results, no practical implementations have achieved the desired level of tunability or addressed issues like scalability, fabrication complexity, and reliability under operational conditions. The ongoing development of advanced fabrication technologies and novel material systems is crucial to overcoming these obstacles and realizing the full potential of graphene/dielectric metasurfaces in next-generation photonic devices.

3. Lenses, graphene metasurfaces-based lenses and fabrication methods

3.1. Lenses

Lenses are constructed from materials characterized by distinct electromagnetic properties and geometrical configurations to regulate the propagation of electromagnetic waves [55,56]. Electromagnetic lenses are available in several types: (1) Dielectric lenses made of glass or plastic of relatively high refractive index. These devices work on the principle of refraction, wherein the change in speed of light changes its course of movement as it passes through the lens. Dielectric lenses are frequently used in optical systems like cameras and microscopes [57–59]. (2) Graded index lenses feature a refractive index that gradually changes across their surface, unlike traditional lenses with a constant index. This gradual variation allows them to focus light without requiring complex optical elements, resulting in simpler and more compact lens designs [60–64]. (3) Metalenses, also known as metasurface lenses, are flat lenses composed of nanostructures, typically arranged in periodic patterns. These nanostructures interact with incoming light waves to manipulate their phase, allowing for precise control over the direction and focus of light. By leveraging metasurface technology, these lenses can perform unconventional wave manipulations, such as achieving a negative refractive index or enabling super-resolution imaging. Their compactness and advanced functionality make them significant for miniaturizing optical systems and enabling new imaging technologies [65–71]. The third classification, referred to as lens arrays, not only demonstrates focusing incoming wave and imaging capabilities but also reveals a variety of captivating attributes that surpass those associated with single lenses. Lens arrays find widespread application in areas such as photography, telecommunications, and optical memory [72–77].

For instance, combining a lens array with a Hartmann-Shack sensor offers an effective method for measuring wavefronts at visible light wavelengths [78]. Furthermore, lens arrays are broadly utilized in cameras to enhance the quality of the images [79–81]. These lens arrays are crucial in various applications of terahertz imaging systems and communication technologies. Generally, each lens is paired with a terahertz detector to enable pixel detection. Additionally, lens arrays with adjustable focal lengths can be used in two-dimensional and three-dimensional displays and tunable photonic devices. Applying an external voltage to graphene modifies its carrier density, which in turn alters its optical conductivity and refractive index, enabling precise tuning of the focal point [82–84]. However, their conventional preparation through laser direct writing in optical and silicon machining methods is complex and expensive. Such processes require intricate connections, storage systems, and photovoltaic imaging [85].

Lenses enabled by metasurface technology pave the way for innovative designs of planar terahertz devices, with promising applications in terahertz imaging and communications [86,87]. As mentioned, metasurfaces based on metallic or dielectric materials are passive and non-tunable. However, graphene-based metasurfaces offer a distinct advantage: the possibility to change the lens pattern or phase distribution without actually changing the structure. Therefore, we will explore some of these lens models.

3.2. Graphene metasurfaces-based lenses

This section investigates various graphene metasurface-based lenses and discusses some associated challenges. Ref [88] describes a cutting-edge optical device designed for precise beam steering at the telecommunications wavelength of 1550 nm. This device features a reflective metalens paired with five switchable nano-antennas, while a graphene-based switchable power divider manages incoming light flow. To achieve high angular accuracy in the emitted beams, the author employs a novel holographic algorithm that aligns the feeding nano-antennas optimally with the metalens. An additional algorithm selects the most suitable unit cells within the metalens to maintain consistent light intensity during beam rotation, supporting efficient and stable performance. Together, these innovations represent a substantial leap in optical device technology, offering enhanced applications in telecommunications.

Ref [89] illustrates a programmable graphene metasurface inspired

by quantum effects that has been designed to achieve electromagnetically generated transparency. Adjusting the DC voltages applied to graphene sheets allows the cross-polarized transmission of each array's amplitude and phase to be continuously tuned, enabling switching between 0 and 180°. Adaptable control of radiation angles and focal lengths for THz beams can be an important result of this adjustability, supporting diverse manipulation across both amplitude and phase domains. Fig. 1(a) illustrates the programmable graphene metasurface, highlighting its capability to control THz propagation using unified line electrodes. The detailed configuration of the fundamental unit cell is shown in Fig. 1(b).

A versatile flat lens designed to reflect the visible and near-infrared bands has been proposed in Ref [90]. This design integrates a hybrid graphene-metasurface structure with switching capabilities. A dual-purpose device that can alternate between reflective and absorptive states is essential to enable this functionality. This approach involves using a gold substrate featuring two opposing slits to generate an absorption mechanism, while a graphene layer is utilized to control the intensity of both absorption and reflection. The capability to toggle between these states for incident light with circular polarization is accomplished by equally modifying the μ_c of the graphene sheet. When the chemical potential of graphene, denoted as μ_c, is established at 1.1 eV, the device exhibits reflective properties. This reflective state demonstrates a broad optical response ranging from 715 to 800 nanometers, with a polarization conversion efficiency exceeding 70 percent. Conversely, setting μ_c to 0.75 eV results in absorptive characteristics within the wavelength range of 700 to 780 nanometers. In addition to developing adjustable flat lenses with single and dual focusing, a multifunctional configuration capable of transitioning between various modes, including unfocused, single-focus, and dual-focus modes, has been introduced. These adjustable flat lenses show promise for diverse imaging and sensing systems applications. Fig. 2(a) presents a direct schematic of the proposed flat lens, which includes a TiO_2 nanofin positioned above a graphene layer on a gold mirror substrate with slits. Fig. 2(b) illustrates a representation of the operation of a flat lens with reflective focusing based on a metasurface. The reflected wave can be precisely focused at a selected location above the structure using an optimized phase profile. This ideal phase profile (denoted as phi subnormal) in Fig. 2(c) corresponds to a focal distance of $z = 5$ Âμm and a wavelength of 740 nanometres. The phase characteristics of the flat lens are determined by varying the angle of orientation θ of the nanofins. Additionally, Fig. 2(d)-(e) shows the top and front views of the proposed flat lens with single-point focusing, respectively. Furthermore, Fig. 2 (g)-(i) displays the normalized intensity cross-section at the center focal point along the x and y directions.

In [91], a novel approach using digital graphene-based metasurfaces is introduced to manipulate wavefronts' amplitude and phase, addressing challenges within the terahertz (THz) range. These metasurfaces consist of digital building blocks, allowing direct digital data modulation by choosing specific digital sequences and transmitting them to targeted receivers at focal points. A multi-channel, high-speed THz communication system is subsequently presented, aimed at enabling three-dimensional wireless agile interconnection. Additionally, in [92], another lens design is proposed, featuring a graphene-based metasurface in a ring configuration with double oblique gaps and four curved channels. When exposed to incident waves at 632.8 nm, surface plasmon polaritons (SPPs) produced within the oblique gaps interact with the curved channels, creating varied phase delays at different positions. These SPPs propagate towards a distant focal point, producing a spatial focusing effect with a measured focal length of 2.7 μm and a full height at half maximum of 284 nm.

3.3. Fabrication methodes

The following section will examine various lenses based on graphene metasurfaces, focusing on their fabrication requirements and testing methodologies within the microwave and THz frequency ranges before delving into the specific articles detailing their fabrication methods and experimental results.

Fabrication methods for graphene-based metasurfaces include laser-induced graphene (LIG) for scalable, low-cost THz applications, though it struggles with resolution and uniformity. Chemical Vapor Deposition (CVD) produces high-quality graphene but is expensive and time-intensive. Laser Direct Writing (LDW) allows precise patterning for

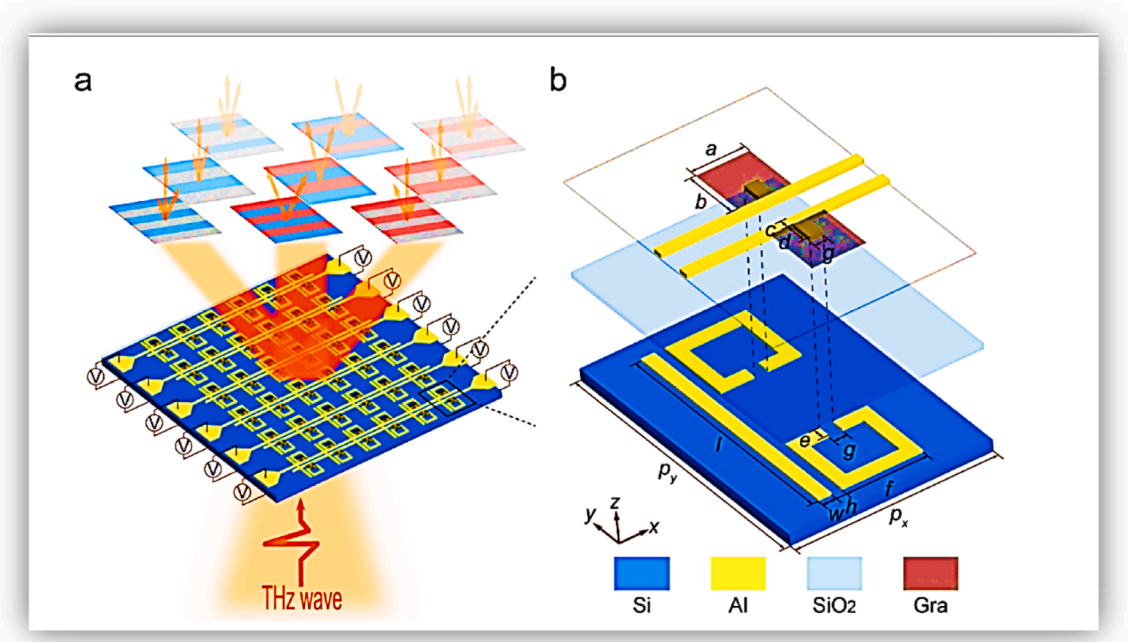

Fig. 1. (**a**) The graphene-based metasurface controlled by two independent DC biases. (**b**) A schematic representation of the basic unit cell illustrates its role within the overall programmable configuration in controlling THz waves effectively (reproduced with permission from [89]).

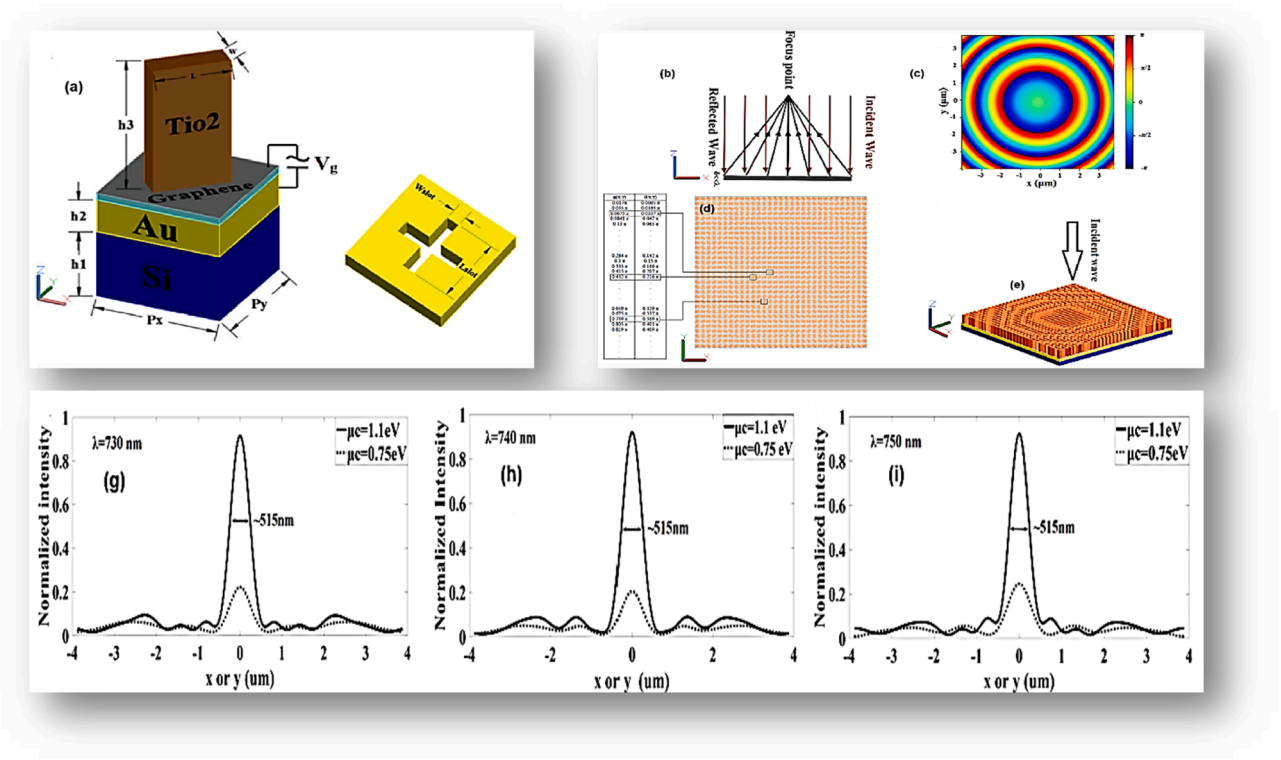

Fig. 2. (**a**) A simplified diagram of the basic structure of the proposed flat lens unit cell. (**b**) An elementary illustration of the reflective flat lens in the suggested design. (**c**) The phase distribution of the lens for light incident at normal angles ensures efficient focusing. (**d**) The top view and (**e**) The front view display the structural layout of the proposed flat lens, optimized for single-spot focusing. (**g**)-(**i**) Normalized intensity cross-sections along the x and y axes highlight the focal spot's center for different graphene chemical potentials, demonstrating tunable focusing capabilities (reproduced with permission from [90]).

flexible lenses but faces challenges with resolution and uniformity. Patterned metal foil growth supports beam reconfiguration for microwaves but suffers from a high loss at these frequencies. Chemical etching enables customizable patterns but risks damaging graphene. Transferring graphene onto substrates like PET creates flexible metasurfaces, though ensuring quality and adhesion is difficult. A combination of CVD and laser etching supports dynamic modulation but is complex with stability issues. Table 1 presents an overview of some of the key fabrication techniques that can be used for graphene-based metasurface lenses. This table highlights various methods, each with its unique features and limitations, providing a foundation for understanding the challenges and advancements in this area of research. Next, we delve into the fabrication methods of various graphene-based metamaterials and metasurfaces in greater detail.

In [93], a graphene-based metamaterial was designed and fabricated using a tightly focused femtosecond laser beam, demonstrating promising results with this fabrication method [94]. The fabrication of the metamaterial involves three main steps: deposition of the silver mirror and SiO_2 spacer onto a substrate, self-assembly of Graphene Oxide (GO) and dielectric multilayers, and the reduction of GO followed by grating fabrication using femtosecond laser writing.

The silver mirror and SiO_2 spacer layer are deposited via physical vapor deposition. The graphene-based metamaterial layer is created through the wet chemical self-assembly method, where negatively charged GO layers and positively charged poly-diallyldimethylammonium chloride (PDDA) are alternately deposited due to electrostatic forces43. The selection of the dielectric material controls the dielectric layer thickness, while the thickness of GO layers is regulated by the concentration of the GO solution and the thickness of GO flakes, typically 1–2 layers. The thickness of each layer and surface roughness are measured using an atomic force microscope. A consistent 2-nm thickness for GO layers is achieved, and the surface roughness is maintained below 2 nm, which is critical for photonic applications.

The grating is fabricated using a tightly focused femtosecond laser beam38. A λ=800 nm laser with 100 fs pulses, focused through a 0.8 numerical aperture (NA) objective lens, is used. The laser beam also partially reduces the GO layers. The removal of oxygen-containing groups and the restoration of the sp^2 graphene network are confirmed via X-ray photoelectron spectroscopy (XPS) spectra. As the photothermal effect drives the photo-reduction, the degree of reduction is finely adjustable with laser power. At higher power levels (approximately 60 μW in this study), the GO layers are transformed into graphene-like material with nearly completely removing oxygen-containing groups. During this process, the 2-nm-thick GO layers are reduced to approximately 1-nm-thick graphene layers as the atomic spacing decreases from 8.1 Å for GO to 3.4 Å for graphene.

In [95], a graphene/gold bilayer metasurface is fabricated using the CVD method. The fabrication of the graphene/gold bilayer metasurface is centered on integrating precision and scalability to achieve a functional device. The process begins with the preparation of a flexible Rogers 5880LZ laminate substrate. Gold layers are deposited on both sides, with one side serving as an RF ground and the other defining the metasurface area and contact regions using a hard mask. High-quality graphene films, synthesized through a CVD process on a Nickel catalyst, are transferred onto the substrate using a wet transfer technique to ensure strong adhesion and minimal residue.

The graphene/gold bilayer is then patterned into a specific metasurface design using photolithography, involving the application and development of photoresist layers. Reactive ion etching is used sequentially with oxygen and argon plasmas to precisely remove unprotected regions of graphene and gold. Electrical connections are established with silver epoxy, completing the structure. This fabrication approach enables the creation of a highly tuneable, well-defined metasurface, ideal for advanced terahertz applications. Fig. 3(a)-(d) shows the schematic of the unit cell and its fabricated structure.

Next, we will review several articles on the fabrication of graphene-

Table 1
Fabrication methods of graphene-based metasurface lens.

Fabrication Method	Key Features	Limitations
Laser-Induced Graphene (LIG)	Scalable and low-cost; rapid production with high resolution for THz metasurfaces. . Ideal for large-scale production because of scalability and simplicity of Operation.	Limited resolution; difficulty in achieving uniformity across large areas; primarily suited for THz.
Chemical Vapor Deposition (CVD)	High-quality graphene growth; suitable for complex metasurfaces.	Expensive and time-consuming process; challenges in integrating with other materials.
Laser Direct Writing (LDW)	Allows for precise patterning of graphene oxide for flexible lenses.	Limited by laser resolution and material behavior; challenges with uniformity in stretching.
Growth of Graphene on Patterned Metal Foils	Enables beam reconfiguration in microwave frequency range.	Graphene's high loss at microwave frequencies reduces efficiency; reliance on specific metal patterns.
Chemical Etching (Laser or Conventional)	Customizable graphene patterning for metasurfaces.	Requires precision in etching for functionality; potential for damaging graphene layer during process.
Transfer of Graphene onto Substrates (e.g., PET)	Suitable for creating thin and flexible metasurfaces. Ideal for large-scale production because of scalability, material compatibility and adaptability for flexible electronics.	Difficulties in ensuring high-quality graphene transfers; alignment and adhesion challenges.
CVD & Laser Etching Combined	Enables dynamic amplitude and phase modulation at microwave frequencies.	High fabrication complexity; potential issues with material stability and reproducibility.

based metasurface lenses. The challenge of achieving comprehensive control over the wavefront at microwave frequencies arises primarily from the difficulty in obtaining complete phase coverage of 2π with equal amplitudes using graphene. However, the requirement for a binary-phase distribution with a π phase difference in the 1-bit coding metasurface greatly improves the practicality of using graphene for wavefront manipulation. This concept is inspired by coding metasurfaces. Research conducted by Chen et al. [96] explored the restructuring of microwave beams using graphene ribbons, revealing strong consistency between experimental and simulated results. However, these designs did not demonstrate true dynamic reconfigurability. Subsequently, programmable graphene metasurfaces were experimentally introduced in 2020, achieving dynamic wavefront shaping [97]. The microwave programmable graphene metasurface (MPGM) was developed and experimentally validated. The conditions for creating a binary element with resistive materials were established through equivalent impedance analysis. Based on this analysis, the reflection amplitude and phase can be attained by adjusting the biasing applied to the graphene sheet. Furthermore, the metasurfaces allow for independent control over different elements. Both simulations and experimental results indicate that the MPGM can perform various functions, including beam redirection and radar cross-section reduction. This development marks a significant advancement in applying graphene to adjust phase amounts within the microwave frequency range. However, a notable limitation of this study is that metallic structures and the resonance of patterned graphene constrain the binary-phase response. In this context, the reflection is relatively weak (approximately 0.3) due to the high loss associated with graphene in the microwave spectrum. Following a similar strategy, Zhang et al. [98] proposed another promising method to independently regulate amplitude within the phase coding metasurface for dynamic wavefront manipulation at microwave frequencies. A prototype of a metasurface-based metal slab comprising "0″ and "1″ grids arranged in an optimized encoding arrangement was constructed using standard printed circuit board (PCB) techniques. The layer includes 32 × 32 meta-elements printed on a 1.524 mm thick Rogers RO4350B substrate. A layer of graphene sheet was also created on an 18-micron-thick copper sheet through chemical vapor deposition (CVD). This graphene layer was transferred onto a 75-micron-thick PET substrate via a layering and etching process. Subsequently, the metasurface-based graphene sheet was engineered using a normal laser beam-cutting method.

Another significant application of lenses is in imaging; however, achieving adjustable color imaging across the full visible spectrum poses

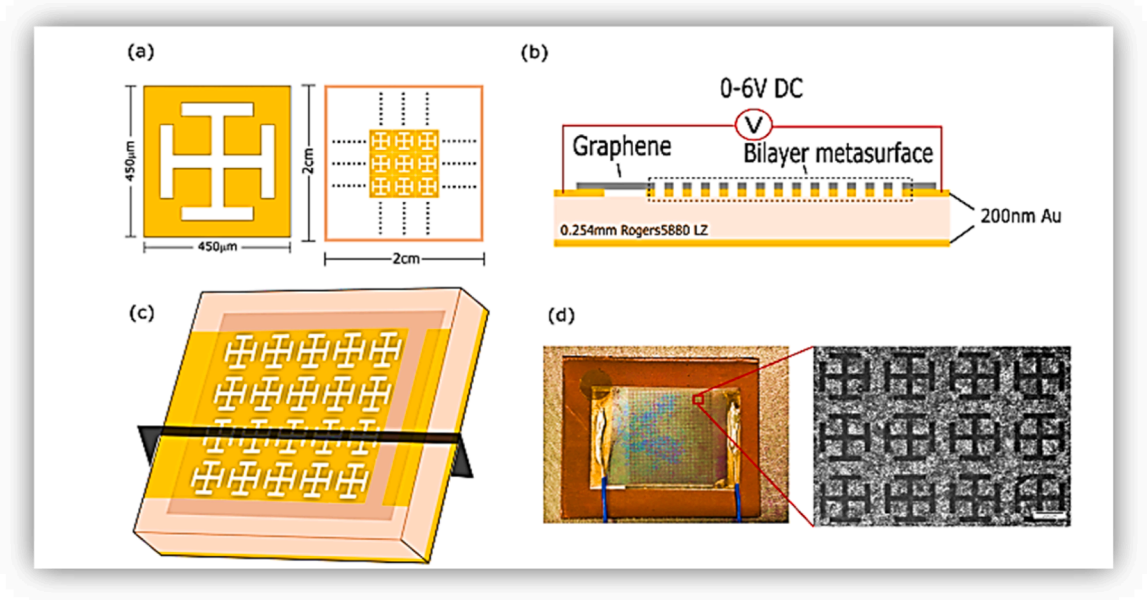

Fig. 3. (**a**) Dimensions and array structure of the Jerusalem-cross-slot unit cell. (**b**) Cross-sectional view of the graphene/gold bilayer superimposed metasurface structure, as indicated by the intersecting black plane in (**c**). (**c**) Schematic of the 0.2 THz frequency-selective absorber device. (**d**) Fabricated bilayer device with a zoomed-in optical image highlighting the well-defined metasurface structure (reproduced with permission from [95]).

practical challenges. Fig. 4(a)-(e) and Fig. 5(a)-(i) show the shape of the unitcell, fabricated structure and its results. In response, Shibiao Wei and colleagues [99] proposed and experimentally demonstrated a broadband and variable-focal-length lens made of graphene, with a thickness of only 250 nanometers, encompassing the entire visible range. This lens facilitates continuous adjustment of the focal length for multiple wavelengths simultaneously. By applying lateral strain, up to 20 percent of the focal length adjustment range was achieved for red (650 nm), green (550 nm), and blue (450 nm) light, indicating three distinct wavelengths. Adjusting the graphene-metal strain ratio enabled effective zoom imaging of items positioned along the optical axis for these wavelengths. This progress paves the way for small imaging devices like smartphones, wearable displays, and miniaturized communication systems, offering multichannel Spectrum capabilities. Fig. 6(a)-(i) illustrates the fabrication of stretchable Graphene Oxide (GO) metals and their imaging capabilities, while Fig. 7(a)-(e) displays the results of 3D imaging and focal length adjustment achieved using stretchable graphene metals.

A graphene-based metasurface lens fabrication method is introduced in [46], leveraging laser-induced graphene (LIG) for THz wave modulation due to its high conductivity. The study presents an efficient LIG fabrication process utilizing a nanosecond laser, a telecentric scan lens, and scanning mirrors. This setup allows for rapidly producing a THz metasurface (15 mm by 15 mm) with 30 μm resolution in just 34 s, offering a scalable and cost-effective solution.

The schematic of the LIG fabrication system, shown in Fig. 8, illustrates its main components. These include a Nd:YVO4 nanosecond solid-state laser (pulse width: 15 ns, adjustable repetition rate) with an output wavelength of 532 nm, a beam expander, a telecentric scan lens with a focal length of 60 mm, and a scanning system. The scanning system consists of two mirrors capable of tilting the laser beam in the x- and y-directions. Through a controlling system, the focused laser beam is swept across a 2D plane to produce LIG patterns.

Commercial Kapton PI tape, with a thickness of 80 μm, is employed as the carbon precursor and adhered to a 1 mm-thick quartz glass substrate, which exhibits high THz wave transmittance.

In contrast to traditional LIG fabrication systems utilizing a two-dimensional translation stage, scanning mirrors offer the benefit of faster laser beam tilting. However, for large deflection angles, the focal spot becomes elliptical, reducing fabrication resolution. To address this issue, a telecentric scan lens with a 60 mm focal length and an 18 mm × 18 mm working area is utilized to avoid elliptical distortion. In this area, the focus diameter remains under 5 μm, as detailed in Section S2 of the Supplementary Material. Fig. 9(a)-(b) shows the fabricated structure and its results.

Table 2 provides a detailed explanation of the fabrication methods used for graphene-based metasurfaces and lenses and an overview of their key features. This includes insights into the specific manufacturing processes, such as laser-induced graphene, chemical vapor deposition, and laser etching, as well as the unique characteristics and functionalities of the resulting optical devices, including their tunability, focal length adjustments, and application potential in fields like telecommunications, imaging, and terahertz communication.

4. Challenges of fabrication of graphene metasurfaces-based lenses

However, there are several challenges in the fabrication of graphene metasurface-based lenses, including [100–104]:

4.1. Complexity of fabrication

The fabrication of graphene metasurfaces requires advanced techniques like electron-beam lithography (EBL) and reactive ion etching (RIE) to create precise nanoscale features. EBL enables sub-10-nanometer resolution patterning, while RIE ensures controlled material removal. These methods demand cutting-edge equipment and skilled personnel, significantly increasing production complexity and the risk of defects. Even slight imperfections, such as uneven etching or contamination, can alter key optical properties, affecting device performance.

Efforts to enhance scalability and reduce defects include alternative techniques like nanoimprint lithography and post-fabrication corrections, aiming to balance precision with large-scale manufacturing feasibility. These improvements are crucial for realizing graphene metasurfaces' potential in photonic and electronic applications.

4.2. Material contamination

Contamination in graphene materials represents a significant challenge, as even minor impurities can severely impact their optical, electronic, and mechanical properties. These impurities may originate from various sources during the synthesis, processing, or handling stages. Environmental factors such as exposure to airborne dust, moisture, or chemical residues are common culprits. Additionally, impurities might be introduced from synthesis equipment, storage containers, or external reactive agents used during fabrication.

The presence of these contaminants can alter graphene's atomic structure and disrupt its electronic band configuration, negatively affecting critical characteristics such as electrical conductivity, carrier mobility, and optical transparency. For instance, contaminants may interfere with the movement of electrons through the graphene lattice,

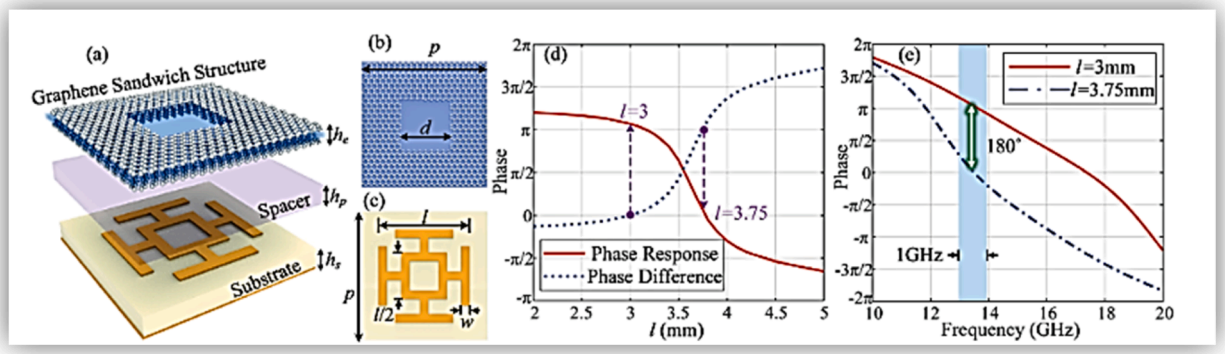

Fig. 4. (**a**) A 3D schematic representation of a meta-atom. (**b**) Top view of the unit cell of the graphene layer. (**c**) Top view of the unit cell of the metal pattern layer. (**d**) The relationship between the reflected phase and the structural parameter *l*. (**e**) The reflected phase of "0″ and "1″ elements as a function of frequency (reproduced with permission from [98]).

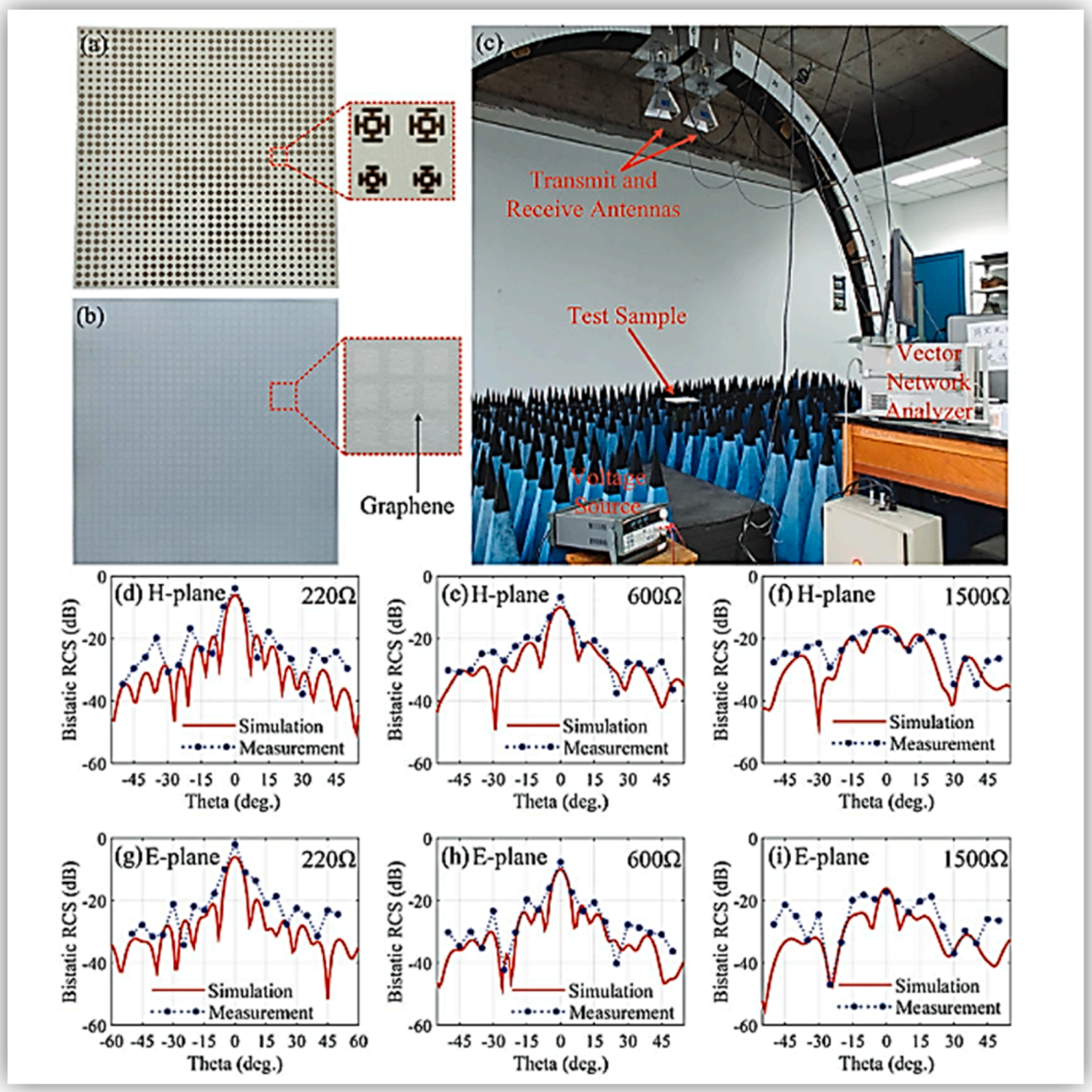

Fig. 5. (**a**) The metal-patterned layer, (**b**) The graphene-patterned layer, and (**c**) The measurement setup. (**d–i**) Bistatic RCS of the designed coding metasurface at 13.3 GHz in the H-plane and E-plane, corresponding to R_g values of 220 Ω, 600 Ω, and 1500 Ω, respectively (reproduced with permission from [98]).

leading to increased resistance and degraded performance in applications like photodetectors, transparent conductive films, or optical lenses. Contamination can also influence graphene's interaction with light, causing deviations in light absorption, reflection, or transmission, which are crucial in optoelectronic applications.

Maintaining high purity in graphene materials is paramount to preserving their exceptional properties and achieving the desired performance in graphene-based devices. Rigorous synthesis protocols, cleanroom environments, and precise handling measures are often implemented to minimize contamination. For advanced applications, post-synthesis purification techniques, such as chemical treatments or thermal annealing, are frequently employed to ensure that graphene meets the stringent purity requirements necessary for high-efficiency photonic, electronic, and optical systems.

4.3. Financial considerations

The economic aspects of producing and refining high-quality graphene are significant hurdles in advancing its commercial viability, especially for applications like lenses. The costs associated with the raw materials, sophisticated fabrication techniques, and stringent quality control measures can accumulate rapidly. Additionally, scaling up production to meet commercial demands while maintaining quality standards often leads to further financial burdens. This high cost of entry can deter potential investors and slow the widespread adoption of graphene technologies in various industries, from optics to electronics.

4.4. Adjustment and regulation

Achieving precise control over the optical attributes of graphene metasurfaces is a highly challenging task, necessitating sophisticated

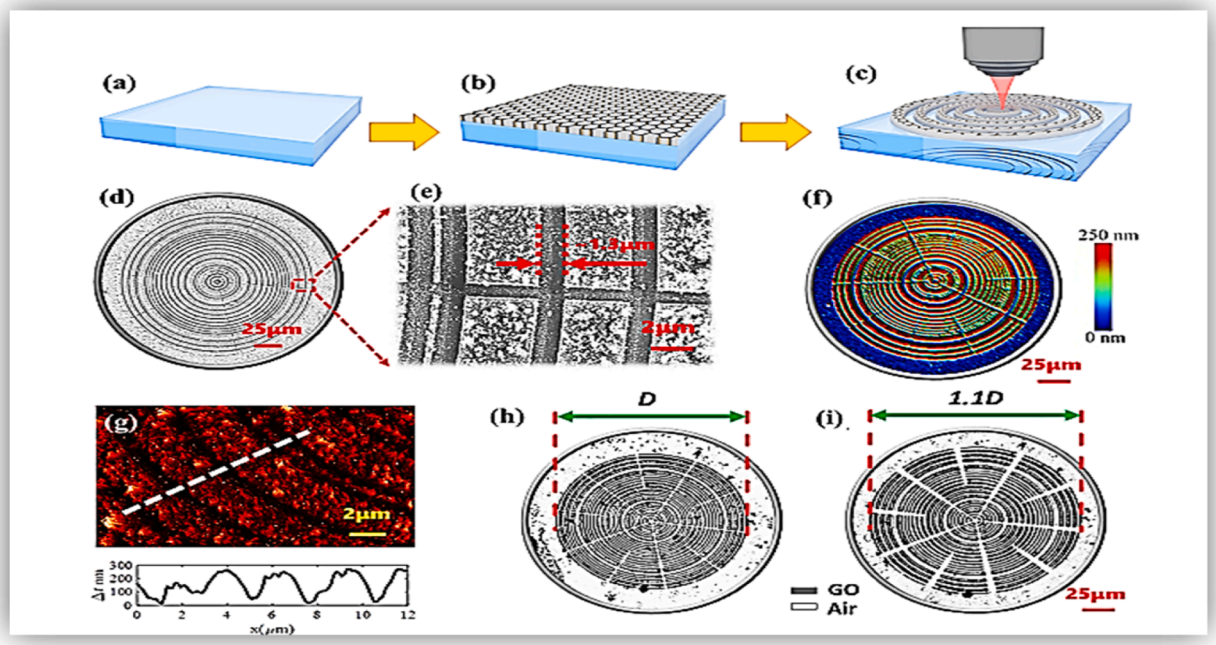

Fig. 6. Fabrication and imaging of flexible Graphene Oxide metalenses: (**a-c**) Steps in creating graphene metalenses: (**a**) Preparation of the PDMS substrate. (**b**) Transferring the Graphene Oxide sheet onto the PDMS substrate. (**c**) Formation of graphene metalenses via laser direct writing. (**d-e**) Images of the metalens show an air ring width of 1.3 Âµm . (**f**) View of the lens. (**g**) The lens's surface structure, with the lower curve illustrating. (**h**) Bright-field optical image of the lens in the unstretched state, where the gray part represents the Graphene Oxide region, and the white part shows the laser-removed Graphene Oxide. Thin radial airlines were added around the Graphene Oxide ring to enable stretching. The main lens diameter was 150 Âµm (D). (**i**) Bright-field optical image of the metalens after uniform stretching, with a stretch ratio of 1.1 (reproduced with permission from [99]).

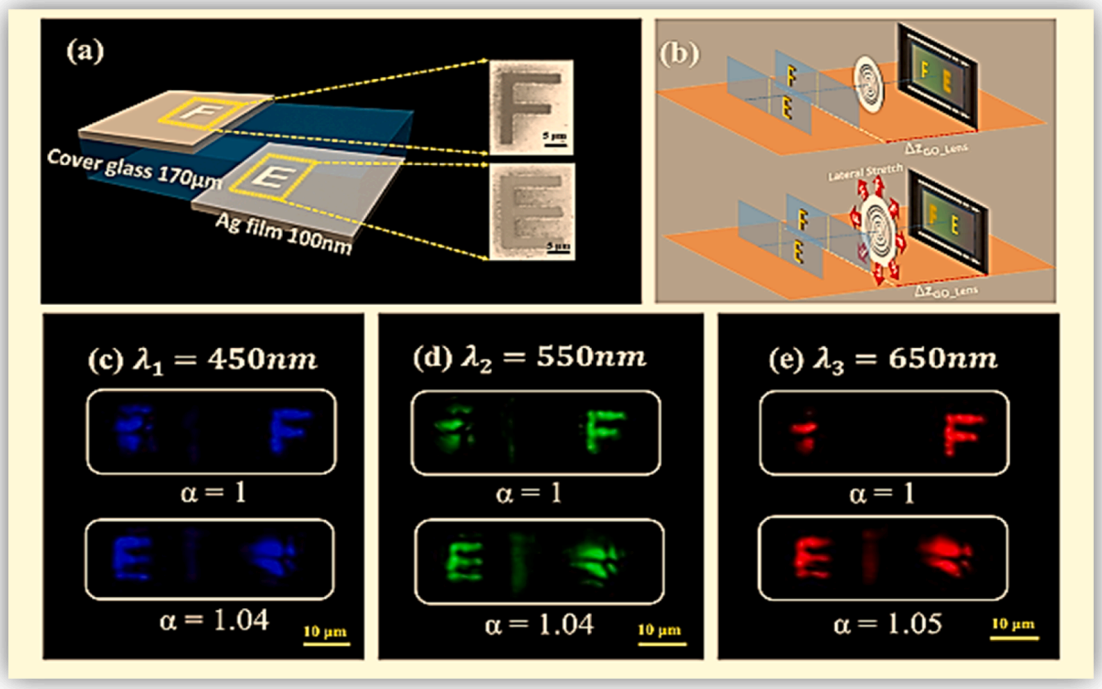

Fig. 7. 3D targeting and variable focal length imaging with a flexible graphene lens. (**a**) The inset images display reflections of laser-fabricated objects "E" and "F," with a line width of 2 Âµm and a height of 18 Âµm . A 100 nm layer of silver was covered on both faces of glass with a 170-micrometer thickness. (**b**) Stretching the flexible graphene lens enabled sharp imaging of objects at different field depths, as illustrated in the zoom imaging schematic. (**c, d, and e**) Zoom imaging for blue, green, and red light under various extend ratios (reproduced with permission from [99]).

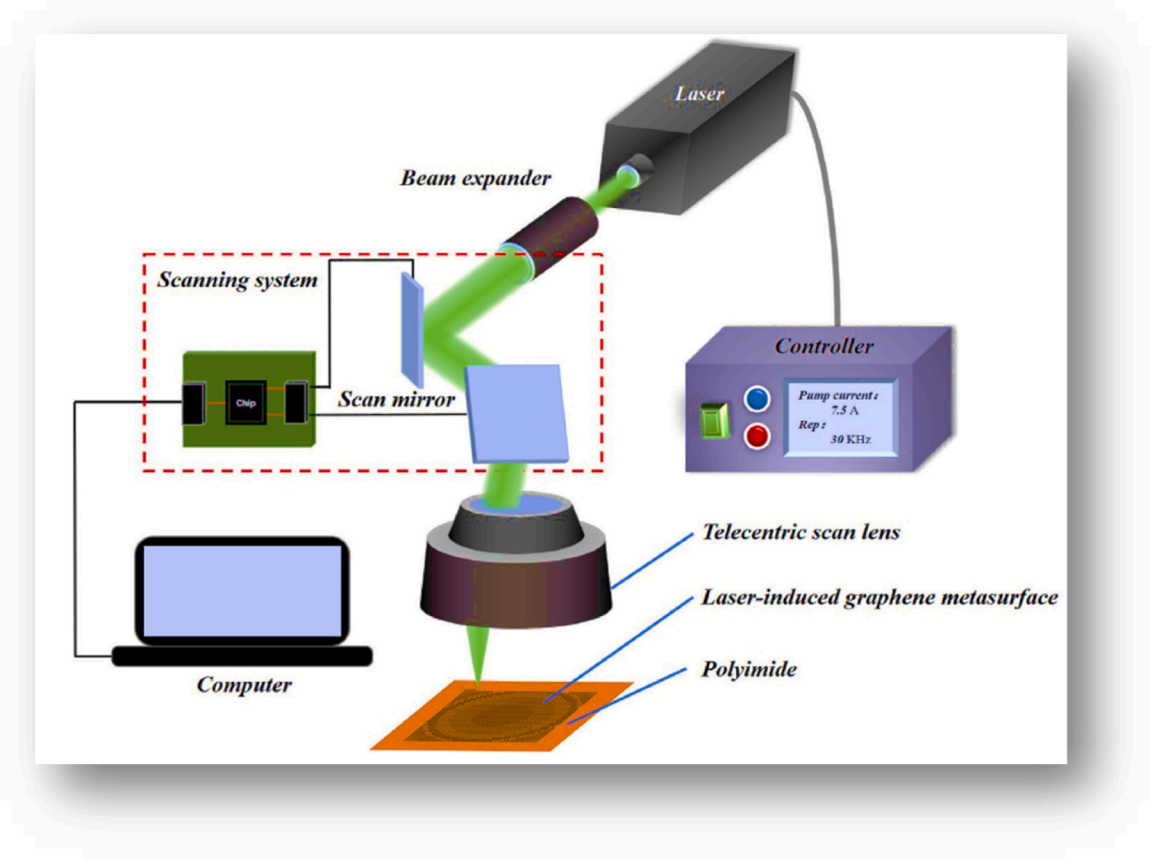

Fig. 8. The Schematic of the fabrication setup (reproduced with permission from [46]).

and accurate tuning mechanisms. These metasurfaces are designed to manipulate properties such as phase, amplitude, polarization, and wavelength-specific interactions of light, which require dynamic and responsive adjustment to external stimuli. Common stimuli include electric fields, magnetic fields, temperature variations, mechanical strain, or chemical doping. Each of these factors introduces unique technical demands on the metasurface design and integration process.

For example, the use of electric fields to adjust optical properties requires careful consideration of electrode placement, field strength, and uniformity to ensure consistent performance across the metasurface. Similarly, magnetic field-based tuning demands precise control over field orientation and intensity, while temperature-dependent mechanisms necessitate the use of thermally robust materials and designs capable of rapid heat dissipation or regulation. Strain engineering, often employed to fine-tune graphene's electronic and optical characteristics, adds further complexity by requiring meticulous control of mechanical deformations without damaging the material.

The necessity for real-time or near-instantaneous responsiveness adds an additional layer of challenge. Any delay, instability, or inaccuracy in the tuning mechanisms could result in significant performance degradation, especially in applications where high precision is crucial, such as in beam steering, holography, adaptive optics, and sensors. This demands not only precise engineering but also robust testing and validation of the metasurface under different operating conditions to ensure reliability and repeatability.

Furthermore, the integration of these dynamic tuning systems often involves a trade-off between complexity, fabrication cost, and device scalability. For instance, adding more advanced tuning mechanisms can make the system more versatile but also more difficult to manufacture on a large scale. Designers must carefully balance these factors while maintaining the metasurface's intended functionality and optical efficiency.

Addressing these challenges often involves the development of innovative material designs and hybrid systems that combine graphene metasurfaces with other technologies, such as plasmonic structures or dielectric substrates, to enhance their responsiveness and minimize losses. Collaborative advancements in fabrication techniques, material science, and computational modelling are critical for overcoming the limitations and realizing the full potential of tunable graphene metasurfaces in cutting-edge photonic and optoelectronic applications.

4.5. Thermal regulation

Thermal management is a vital aspect of the design and operation of graphene metasurfaces, particularly under conditions of intense illumination or high-power optical applications. Excessive heat generation can induce a range of undesirable effects, including thermal expansion, stress within the material, degradation of graphene's intrinsic properties, and alterations in the refractive index of the surrounding substrates. Such thermal effects affect the metasurface's ability to control light precisely and lead to long-term structural and functional deterioration.

Thermal expansion, for example, can distort the precise nanostructures required for the metasurface to manipulate optical properties like phase or amplitude. Similarly, the increase in temperature may modify graphene's conductivity, bandgap characteristics, or plasmonic behavior, thereby compromising its ability to perform efficiently in applications such as beam shaping, sensing, or signal modulation. Accumulated heat could also result in localized damage or delamination of layers, which further diminishes the device's longevity and reliability.

To address these challenges, several thermal management strategies are being explored. One approach is the integration of thermal dissipation systems, such as heat sinks, thermally conductive substrates, or advanced cooling technologies. Materials with high thermal conductivity, such as diamond or boron nitride, can be used as substrates to

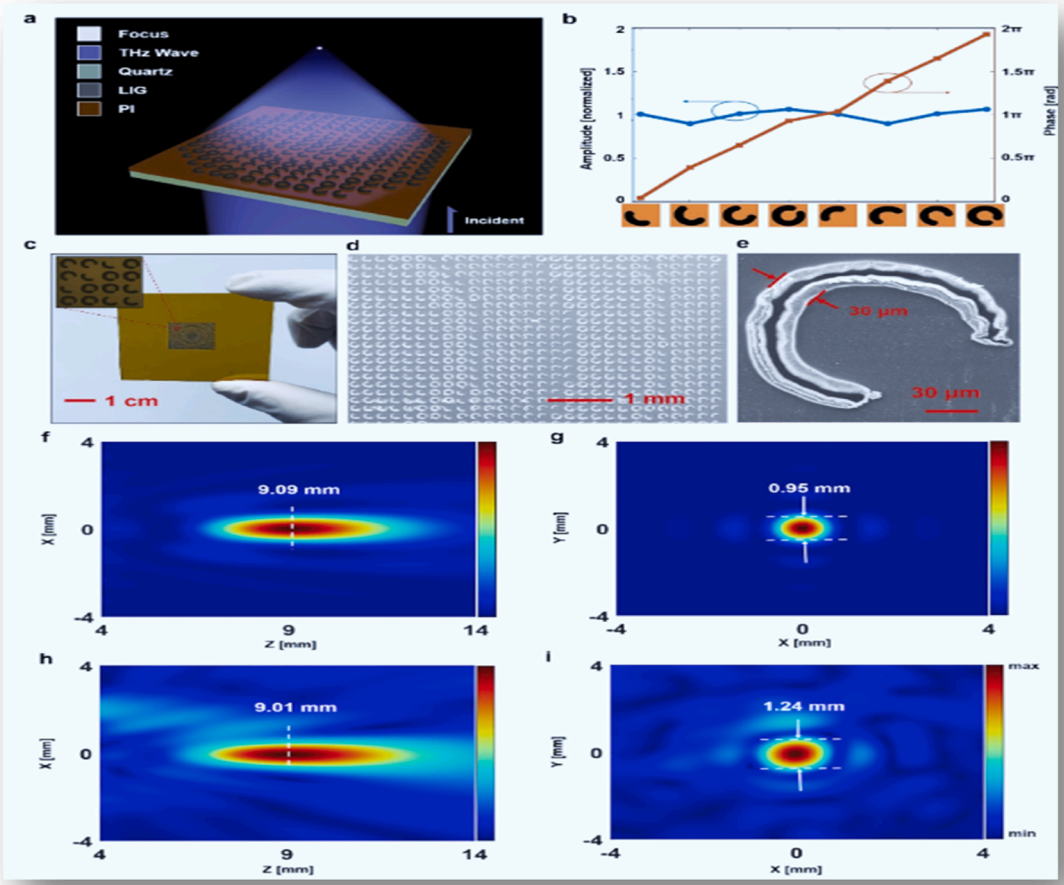

Fig. 9. LIG terahertz metalens utilizing C-shaped antennas. (**a**) Schematic of the LIG terahertz metalens. (**b**) Simulated scattering amplitudes and phases for cross-polarized radiation from 8 different C-shaped antennas. (**c**) Photograph of the terahertz metalens, with the inset showing a microscopic view of the lens. (**d-e**) SEM images of the LIG metalens. (**f**) Simulation results for the intensity distribution of cross-polarized light in the x-z plane. (**g**) Simulated field distribution on the focal plane (x-y plane). (**h**) Experimental results for the intensity distribution of cross-polarized light in the x-z plane. (**i**) Experimental field distribution on the focal plane (x-y plane), with the FWHM indicated in the figures (reproduced with permission from [46]).

effectively transfer heat away from the active graphene layer. Another solution involves the design of metasurface structures that are thermally robust, incorporating materials with low thermal expansion coefficients or high-temperature tolerances to mitigate deformation and property shifts.

In addition to material innovations, optimizing the layout and geometry of the metasurfaces to minimize hotspots or evenly distribute heat can enhance thermal performance. Advanced computational models are often employed to simulate and predict thermal behaviors, enabling designers to implement targeted solutions during the design phase. For applications in demanding environments, such as aerospace or high-power laser systems, the development of hybrid systems that combine active cooling with passive thermal regulation is increasingly being pursued. Effectively addressing thermal regulation is crucial for ensuring that graphene-based metasurfaces maintain their precision and operational integrity over extended periods. By incorporating robust thermal management techniques, these devices can function in high-performance and harsh conditions reliably, unlocking their full potential in cutting-edge photonic and optoelectronic applications.

4.6. Electromagnetic interference

The exceptionally high conductivity of graphene, while beneficial for numerous applications such as high-speed electronics and optoelectronic devices, also poses significant challenges related to electromagnetic interference (EMI). EMI occurs when the electromagnetic fields generated by the conductive graphene interfere with the operation of nearby electronic components. This can manifest as signal distortion, noise, or unintentional coupling between circuits, potentially leading to reduced performance, instability, or even failure of devices incorporating graphene metasurfaces.

The issue becomes particularly critical in complex systems where graphene metasurfaces are used alongside sensitive components, such as in advanced sensors, communication devices, or photonic systems. In such scenarios, the unmitigated generation and propagation of electromagnetic noise can affect the accuracy of measurements, the stability of electronic signals, or the efficiency of optical processes, undermining the intended functionality of the system.

To address these challenges, meticulous design strategies are essential. One approach involves incorporating physical shielding, such as layers of electromagnetic-absorbing materials, to isolate graphene metasurfaces from adjacent components. Shielding can effectively block or attenuate stray electromagnetic fields, reducing their impact on nearby systems. Another strategy is optimizing the spatial layout and orientation of components to minimize the coupling of unwanted signals. For example, strategic placement of metasurfaces in low-interference zones or the use of directional antennas can help reduce noise propagation.

Table 2
Summary of references: fabrication methods and features.

Reference	Fabrication Method	Key Features
[46]	Laser-Induced Graphene (LIG)	A scalable and low-cost method for producing large-area terahertz metasurfaces with rapid, high-resolution fabrication.
[96]	Growing graphene on advanced-patterned metal foils	Demonstrates microwave beam reconfiguration using binary phase coding metasurfaces, suitable for communication and sensing.
[97]	Growing graphene on advanced-patterned metal foils	Enables programmable metasurfaces with binary phase control, tested for wavefront shaping and radar applications.
[98]	Chemical Vapor Deposition (CVD) and Laser Etching	Utilizes a metal slab-based metasurface for dynamic amplitude and phase modulation, highlighting applications in optical devices.
[99]	Laser Direct Writing of Graphene Oxide	Introduces a stretchable graphene metalens capable of variable focal length and zoom imaging in the visible spectrum.
[104]	chemical vapor deposition (CVD)	This groundbreaking graphene-based ultrathin square subpixel lens (USSL) introduces a paradigm shift in display technology, offering pixel-scale, electrically tuneable focusing with unprecedented efficiency and versatility for next-generation multifunctional displays.

Advanced algorithmic solutions are also being explored, including the development of signal processing techniques that can identify and filter out interference in real-time. These algorithms, often powered by machine learning, can differentiate between functional signals and noise, ensuring reliable operation even in electromagnetically complex environments. Additionally, the use of hybrid materials that combine the advantages of graphene with inherent EMI shielding properties, such as graphene-polymer composites, is gaining attention as a material-level solution to EMI challenges.

Addressing these challenges is critical for the seamless integration of graphene metasurfaces into complex electronic and photonic systems. By implementing comprehensive mitigation techniques, it becomes possible to harness the unique advantages of graphene without compromising the stability or performance of surrounding components. This effort is especially vital in high-precision or mission-critical applications, such as medical devices, aerospace systems, and advanced telecommunications networks, where reliability and signal fidelity are of utmost importance. Table 3 highlights the mentioned challenges and their solutions for better readability.

Table 3
Challenges of fabrication of graphene metasurface-based lenses.

Challenge	Description	Solutions/Strategies
Complexity of Fabrication	Advanced techniques like EBL and RIE are required for nanoscale precision. These methods are costly, complex, and require skilled personnel. Defects or uneven processing can affect optical properties.	Explore alternative methods, such as nanoimprint lithography, and implement post-fabrication corrections. Focus on balancing precision with scalability.
Material Contamination	Synthesis, processing, or handling impurities affect graphene's optical and electronic properties. Contaminants disrupt conductivity and optical clarity.	Maintain cleanroom environments and implement purification techniques such as chemical treatments or thermal annealing to ensure high material purity.
Financial Considerations	High production costs stem from expensive raw materials, advanced equipment, and quality control demands. Scaling up for commercialization increases costs.	Optimize fabrication methods, improve scalability, and leverage partnerships or incentives to make graphene production more cost-effective.
Adjustment and Regulation	Precise tuning of optical attributes requires responsive mechanisms driven by external stimuli, increasing complexity and system demands.	Use hybrid designs that combine graphene with complementary technologies, enhanced computational models, and robust testing under varied conditions.
Thermal Regulation	Heat generated during operation leads to thermal expansion, degradation, or structural stress, reducing long-term reliability.	Integrate heat sinks or thermally conductive substrates and design robust structures to manage thermal effects efficiently.
Electromagnetic Interference (EMI)	Graphene's conductivity can cause EMI, disrupting neighboring components and affecting system performance.	Implement physical shielding, optimize layouts, and develop EMI mitigation algorithms. Use hybrid materials with inherent EMI shielding capabilities.

5. Conclusion

In conclusion, developing lenses utilizing graphene metasurfaces offers a promising direction for improving optical technologies. These lenses provide unprecedented control over light propagation, facilitating functions like focusing, beam shaping, and polarization manipulation with exceptional precision and efficiency. Nonetheless, several challenges must be addressed to exploit the potential of graphene metasurfaces in practical scenarios fully. Fabrication intricacy, material impurities, and cost remain key challenges in realizing high-performance graphene metasurface lenses. Achieving perfect calibration and regulation of optical properties, minimizing thermal effects, and overcoming electromagnetic interference is particularly challenging. Despite these hurdles, research on graphene metasurface technology has continued, investigating inventive solutions and pioneering manufacturing techniques to overcome the limitations. As advancements in material science, nanofabrication, and optical engineering converge, graphene metasurface-enabled lenses hold great potential to revolutionize applications like imaging, sensing, communications, and photonic integration. The future of graphene metasurfaces influencing optics would appear only slightly more realizable if the set of advanced multidisciplinary collaboration continued and the investigation was, after all, unrelenting.

Data availability

Data underlying the results presented in this paper are not publicly available at this time but may be obtained from the authors upon reasonable request.

Funding

This work was supported by the Australian Research Council - ARC Linkage Projects (LP210300004).

CRediT authorship contribution statement

Meisam Esfandiari: Writing – review & editing, Writing – original draft, Visualization, Validation, Software, Resources, Project administration, Methodology, Investigation, Formal analysis, Data curation, Conceptualization. **Xiaojing Lv:** Writing – review & editing, Writing – original draft, Visualization, Validation, Supervision, Software, Resources, Project administration, Methodology, Investigation, Formal

analysis, Data curation, Conceptualization. **Shaghayegh Chamani:** Writing – review & editing, Writing – original draft, Visualization, Validation, Software, Resources, Project administration, Methodology, Investigation, Formal analysis, Data curation, Conceptualization. **Yang Yang:** Writing – review & editing, Writing – original draft, Visualization, Validation, Supervision, Software, Resources, Project administration, Methodology, Investigation, Funding acquisition, Formal analysis, Data curation, Conceptualization.

Declaration of competing interest

The authors declare no conflicts of interest related to this work and confirm the absence of any personal relationships that could have influenced the research presented in this paper.

Acknowledgements

The author declares there are not any known competing financial interests or personal relationships that could have appeared to influence the work reported in this paper.

Supplementary materials

Supplementary material associated with this article can be found, in the online version, at doi:10.1016/j.mtelec.2025.100140.

Data availability

No data was used for the research described in the article.

References

[1] A.K. Geim, K.S. Novoselov, The rise of graphene, Nat. Mater. 6 (3) (2007) 183–191, https://doi.org/10.1038/nmat1849.
[2] Anindya Nag, et al., Graphene-based wearable temperature sensors: a review, Mater. Des. 221 (2022) 110971.
[3] Aishani Sharma, et al., Novel SolidStir extrusion technology for enhanced conductivity cable manufacturing via in-situ exfoliation of graphite to graphene, Mater. Des. 238 (2024) 112643.
[4] Chen Chen, et al., Numerical study on tunable perfect absorption in square graphene-dielectric arrays at near-infrared wavelengths, Mater. Des. 128 (2017) 157–165.
[5] Elena Bekyarova, et al., Effect of covalent chemistry on the electronic structure and properties of carbon nanotubes and graphene, Acc. Chem. Res. 46.1 (2013) 65–76.
[6] Frederico D. Novaes, Riccardo Rurali, Pablo Ordejón, Electronic transport between graphene layers covalently connected by carbon nanotubes, ACS Nano 4.12 (2010) 7596–7602.
[7] IZZO, Kimi Aki, et al. Graphene based electrode for electrophysiological readings. U.S. Patent Application No 18/251,212, 2023.
[8] Xiwei Zhang, et al., Recent advances in two-dimensional graphitic carbon nitride based photodetectors, Mater. Des. (2023) 112405.
[9] Huihui Zhang, et al., Hybridised graphene for supercapacitors: beyond the limitation of pure graphene, Small 17.12 (2021) 2007311.
[10] Haiyun Yao, et al., Frequency-dependent ultrasensitive terahertz dynamic modulation at the dirac point on graphene-based metal and all-dielectric metamaterials, Carbon. N. Y. 184 (2021) 400–408.
[11] Sushil. Karki, Structural and electronic properties of palladium and palladium doped graphene, Int. J. Sci. Res. Phys. Appl. Sci. 11.5 (2023).
[12] Xintai Wang, et al., Tailoring quantum transport efficiency in molecular junctions via doping of graphene electrodes, J. Mater. Chem. C 12.14 (2024) 5157–5165.
[13] Xin Chen, et al., PAI-graphene: a new topological semimetallic two-dimensional carbon allotrope with highly tunable anisotropic Dirac cones, Carbon. N. Y. 170 (2020) 477–486.
[14] S. Ramirez, et al., Thermal and magnetic properties of nanostructured densified ferrimagnetic composites with graphene-graphite fillers, Mater. Des. 118 (2017) 75–80.
[15] Jun Cai, Ehsan Estakhrianhaghighi, Abdolhamid Akbarzadeh, Functionalized graphene origami metamaterials with tunable thermal conductivity, Carbon. N. Y. 191 (2022) 610–624.
[16] Huan Wang, et al., Deducing the internal interfaces of twisted multilayer graphene via moiré-regulated surface conductivity, Natl. Sci. Rev. 10.8 (2023) nwad175.
[17] F. Bagheri, M. Soroosh, Design and simulation of compact graphene-based plasmonic flip-flop using a resonant ring, Diam. Relat. Mater. (2023) 109904.
[18] Haiyun Yao, et al., Hybrid metasurface using graphene/graphitic carbon nitride heterojunctions for ultrasensitive terahertz biosensors with tunable energy band structure, Photonics Res. 11.5 (2023) 858–868.
[19] Palash Saha, Bala Murali Krishna Mariserla, Unconventional optical response in monolayer graphene due to dominant intraband scattering, Phys. Rev. B 109.12 (2024) 125428.
[20] Zhaoyang Peng, et al., Crystal-momentum-resolved contributions to harmonics in laser-driven graphene, Chin. Phys. Lett. 40.5 (2023) 054203.
[21] Amir Ali Mohammad Khani, et al., Manipulating electromagnetic waves on graphene-based optical device with mixer application: equivalent circuit model approach, Ind. J. Phys. 98.5 (2024) 1827–1832.
[22] Rodriguez-Lopez, Pablo, and Mauro Antezza. "Graphene conductivity: kubo model versus QFT-based model." arXiv preprint arXiv:2403.02279 (2024).
[23] P.S. Tola, P.C. Wardhani, S. Islamiyah, Initial finite-difference time-domain (FDTD) modeling of graphene based on intra-band surface conductivity, J. Phys.: Conf. Ser. 2623 (1) (2023). IOP Publishing.
[24] Mo Liu, et al., Properties of the optical response of the twisted bilayer graphene, Phys. B: Cond. Matter 675 (2024) 415609.
[25] Hao Su, et al., Active control of polarisation-dependent terahertz surface plasmonic wave excitation using coupled graphene-metal hybrid metasurfaces, Phys. Scripta 99.2 (2024) 025526.
[26] Pavlos Mouratidis, James G. McHugh, Kenny Jolley, Modelling of partial basal dislocation dipoles in bilayer graphene and graphite, Carbon. N. Y. 217 (2024) 118613.
[27] Xiaoting Song, et al., Tunable negative permittivity in graphene/poly (vinylidene fluoride) composites with low percolation threshold, Adv. Eng. Mater. 26.2 (2024) 2300203.
[28] Julien Chaste, et al., Nanostructures in suspended mono-and bilayer epitaxial graphene, Carbon. N. Y. 125 (2017) 162–167.
[29] Guiyuan Cao, et al., Multi-wavelength achromatic graphene metalenses for visible, NIR, and beyond, Laser Photon. Rev. (2024) 2401542.
[30] Meisam Esfandiari, et al., Recent and emerging applications of graphene-based metamaterials in electromagnetics, Mater. Des. 221 (2022) 110920.
[31] Gaurav Arya, et al., End-to-end optimization of metasurfaces for imaging with compressed sensing, ACS Photonics 11.5 (2024) 2077–2087.
[32] David A. Katzmarek, et al., Review of graphene for the generation, manipulation, and detection of electromagnetic fields from microwave to terahertz, 2D Mater. 9.2 (2022) 022002.
[33] Meisam Esfandiyari, Saughar Jarchi, Mohsen Ghaffari-Miab, Channel capacity enhancement by adjustable graphene-based MIMO antenna in THz band, Opt. Quant. Electron. 51 (2019) 1–11.
[34] Meisam Esfandiari, et al., Enhancing the sensitivity of a transmissive graphene-based plasmonic biosensor, Appl. Opt. 60.5 (2021) 1201–1208.
[35] Meisam Esfandiyari, et al., Study of a surface plasmon resonance optical fiber sensor based on periodically grating and graphene, Silicon 10 (2018) 2711–2716.
[36] Andrei Andryieuski, Andrei V. Lavrinenko, Graphene metamaterials based tunable terahertz absorber: effective surface conductivity approach, Opt. Express 21.7 (2013) 9144–9155.
[37] Pai-Yen Chen, et al., Graphene-based plasmonic platform for reconfigurable terahertz nanodevices, ACS Photonics 1.8 (2014) 647–654.
[38] Q. Li, Z. Tian, X. Zhang, N. Xu, R. Singh, J. Gu, P. Lv, L.- B. Luo, S. Zhang, J. Han, W. Zhang, Dual control of active graphene-silicon hybrid metamaterial devices, Carbon. N. Y. 90 (2015) 146–153.
[39] Ziqi Miao, et al., Widely tunable terahertz phase modulation with gate-controlled graphene metasurfaces, Phys. Rev. X 5.4 (2015) 041027.
[40] Yuhang Wei, et al., A mid-IR tunable graphene metasurface for ultrasensitive molecular fingerprint retrieval and refractive index sensing, J. Mater. Chem. C 11.47 (2023) 16501–16508.
[41] Bingwei Liu, et al., Ultra-wideband terahertz fingerprint enhancement sensing and inversion model supported by single-pixel reconfigurable graphene metasurface, Photonix. 5.1 (2024) 10.
[42] Cheng Zhang, et al., Graphene-based anisotropic polarization meta-filter, Mater. Des. 206 (2021) 109768.
[43] Chao Zeng, et al., Graphene-empowered dynamic metasurfaces and metadevices, Opto-Electron. Adv 5.4 (2022) 200098.
[44] Boris Luk'Yanchuk, et al., The Fano resonance in plasmonic nanostructures and metamaterials, Nat. Mater. 9.9 (2010) 707–715.
[45] Andrey E. Miroshnichenko, Sergej Flach, Yuri S. Kivshar, Fano resonances in nanoscale structures, Rev. Mod. Phys. 82.3 (2010) 2257.
[46] Zongyuan Wang, et al., Fast-printed, large-area and low-cost terahertz metasurface using laser-induced graphene, Carbon. N. Y. 187 (2022) 256–265.
[47] Yue Wang, et al., Electrically and thermally tunable multifunctional terahertz metasurface array, Phys. Rev. A 105.3 (2022) 033520.
[48] Min Guo, et al., Composite electrode based on single-atom Ni doped graphene for planar carbon-based perovskite solar cells, Mater. Des. 209 (2021) 109972.
[49] Shahram Bahadori-Haghighi, Rahim Ghayour, Abbas Zarifkar, Tunable graphene–dielectric metasurfaces for terahertz all-optical modulation, J. Appl. Phys. 128.4 (2020).
[50] Tian-Yi Zeng, et al., Light-matter interactions enhanced by quasi-bound states in the continuum in a graphene-dielectric metasurface, Opt. Express 29.24 (2021) 40177–40186.
[51] Shengnan Guan, et al., Widely tunable polarisation conversion in low-doped graphene-dielectric metasurfaces based on phase compensation, Opt. Lett. 45.7 (2020) 1742–1745.

[52] Wei Xu, et al., A tunable all dielectric perfect absorber based on hybrid graphene-dielectric metasurface in the mid-infrared regime, Opt. Quant. Electron. 55.3 (2023) 272.
[53] Zheng Zhang, et al., Efficient digital metasurfaces for full-space manipulation of acoustic waves with low crosstalk between reflection and transmission, Mater. Des. 229 (2023) 111903.
[54] Zheng Zhang, et al., Programming reflected and transmitted sound behaviors based on motor-driven digital metasurface, Adv. Funct. Mater. 34.48 (2024) 2411403.
[55] Jiexin Lai, Yang Yang, 3D Printed multifocal lens antenna for terahertz communication, in: *2024 49th International Conference on Infrared, Millimeter, and Terahertz Waves* (IRMMW-THz), IEEE, 2024.
[56] Jiaqi Cai, et al., Additively manufactured wideband millimeter-wave sidelobe suppression of metalens antenna, in: *2023 IEEE International Symposium on Radio-Frequency Integration Technology* (RFIT), IEEE, 2023.
[57] Farizah Ansarudin, et al., Multi beam dielectric lens antenna for 5G base station, Sensors 20.20 (2020) 5849.
[58] Gwan Hui Lee, et al., Wideband high-gain double-sided dielectric lens integrated with a dual-bowtie antenna, IEEE Antennas. Wirel. Propag. Lett. 20.3 (2020) 293–297.
[59] Liang Jiang, et al., Electrohydrodynamic printing of a dielectric elastomer actuator and its application in tunable lenses, Comp. Part A: Appl. Sci. Manuf. 147 (2021) 106461.
[60] Mu Ku Chen, et al., Principles, functions, and applications of optical meta-lens, Adv. Opt. Mater. 9.4 (2021) 2001414.
[61] Jose-Manuel Poyanco, et al., Two-dimensional glide-symmetric dielectric structures for planar graded-index lens antennas, IEEE Antennas. Wirel. Propag. Lett. 20.11 (2021) 2171–2175.
[62] Petros Bantavis, et al., Broadband graded index Gutman lens with a wide field of view utilising artificial dielectrics: a design methodology, Opt. Express. 28.10 (2020) 14648–14661.
[63] Qiao Chen, et al., Double-layer geodesic and gradient-index lenses, Nat. Commun. 13.1 (2022) 2354.
[64] Xavier Porte, et al., Direct (3+ 1) D laser writing of graded-index optical elements, Optica 8.10 (2021) 1281–1287.
[65] Trevon Badloe, et al., Bright-field and edge-enhanced imaging using an electrically tunable dual-mode metalens, ACS Nano 17.15 (2023) 14678–14685.
[66] Xinwei Wang, et al., Single-shot isotropic differential interference contrast microscopy, Nat. Commun. 14.1 (2023) 2063.
[67] Dasol Lee, et al., Hyperbolic metamaterials: fusing artificial structures to natural 2D materials, eLight 2 (2022) 1–23.
[68] Sharon Karepov, Tal Ellenbogen, Metasurface-based contact lenses for color vision deficiency, Opt. Lett. 45.6 (2020) 1379–1382.
[69] Chuan Shen, et al., Metasurface-based holographic display with all-dielectric meta-axilens, IEEE Photonics J. 13.5 (2021) 1–5.
[70] Yuping Shang, Wenjun Zhou, Cheng Liao, Metasurface-based cylindrical lenses and their antenna gain enhancement, Int. J. Antennas. Propag. 2020 (2020) 1–14.
[71] Fangxiao Cheng, et al., Sub-THz 3D printed lens based on diffractive neural network for low-cost detection of orbital angular momentum states, Microw. Opt. Technol. Lett. 65.8 (2023) 2196–2200.
[72] Ji Chen, et al., Planar wide-angle-imaging camera enabled by metalens array, Optica 9.4 (2022) 431–437.
[73] Xiaoyuan He, Li Deng, Yang Yang, 3D-Printed sub-terahertz lens for manipulation of deflective quasi-non-diffractive OAM waves, in: *2021 IEEE Asia-Pacific Microwave Conference* (APMC), IEEE, 2021.
[74] Jianfeng Zhu, Xiaopeng Li, Yang Yang, Conductive and dielectric fully-integrated 3d printed dual-band millimeter-wave fresnel zone plate lens, in: 2021 International Symposium on Antennas and Propagation (ISAP), IEEE, 2021.
[75] Jianfeng Zhu, et al., Additively manufactured millimeter-wave dual-band single-polarization shared aperture fresnel zone plate metalens antenna, IEEE Trans. Antennas. Propag. 69.10 (2021) 6261–6272.
[76] Jianfeng Zhu, et al., Sub-terahertz 3-D printed all-dielectric low-cost low-profile lens-integrated polarization Beam splitter, IEEE Trans. Terahertz. Sci. Technol. 11.4 (2021) 433–442.
[77] Jianfeng Zhu, et al., 3-D printed planar dielectric linear-to-circular polarization conversion and beam-shaping lenses using coding polarizer, IEEE Trans. Antennas. Propag. 68.6 (2020) 4332–4343.
[78] Xiaosong Wu, et al., Study of a Shack-Hartmann wavefront sensor with adjustable spatial sampling based on spherical reference wave, Opt. Lasers. Eng. 160 (2023) 107289.
[79] Mingce Chen, et al., Depth-of-field-extended plenoptic camera based on tunable multi-focus liquid-crystal microlens array, Sensors 20.15 (2020) 4142.
[80] Kristina Monakhova, et al., Spectral DiffuserCam: lensless snapshot hyperspectral imaging with a spectral filter array, Optica 7.10 (2020) 1298–1307.
[81] Sourangsu Banerji, et al., Super-resolution imaging with an achromatic multi-level diffractive microlens array, Opt. Lett. 45.22 (2020) 6158–6161.
[82] Hongtao Wang, et al., Generation of super-resolved optical needle and multifocal array using graphene oxide metalenses, Opto-Electron. Adv. 4.2 (2021) 200031. -1.
[83] Weiguang Liu, et al., Graphene-enabled electrically controlled terahertz metalens, Photon. Res. 6.7 (2018) 703–708.
[84] Ling Li, et al., Broadband polarisation-switchable multi-focal noninterleaved metalenses in the visible, Laser Photon. Rev. 15.11 (2021) 2100198.
[85] Yiyuan Zhang, et al., Bioinspired micro/nanostructured surfaces prepared by femtosecond laser direct writing for multi-functional applications, Int. J. Extr. Manuf. 2.3 (2020) 032002.
[86] Meisam Esfandiyari, et al., Tunable terahertz filter/antenna-sensor using graphene-based metamaterials, Mater. Des. 220 (2022) 110855.
[87] Mahdi Norouzi, et al., 3D metamaterial ultra-wideband absorber for curved surface, Sci. Rep. 13.1 (2023) 1043.
[88] Vahid Ghaffari, Leila Yousefi, Integrated optical beam steering device using switchable nanoantennas and a reflective metalens, Sci. Rep. 13.1 (2023) 7099.
[89] Guanxuan Guo, et al., Programmable graphene metasurface for terahertz propagation control based on electromagnetically induced transparency, Carbon. N. Y. 208 (2023) 345–354.
[90] Amin Araghi, et al., Switchable visible and near-infrared light bifocal lens based on hybrid graphene-metasurface structures, Diam. Relat. Mater. (2024) 110945.
[91] Kasra Rouhi, et al., Multi-channel near-field terahertz communications using reprogrammable graphene-based digital metasurface, J. Lightwave Technol. 39.21 (2021) 6893–6907.
[92] Jinguo Yin, Zhu Jun, Novel tunable graphene-based metasurface of metalens, Optik. (Stuttg) 271 (2022) 170226.
[93] Han Lin, et al., A 90-nm-thick graphene metamaterial for strong and extremely broadband absorption of unpolarized light, Nat. Photonics 13.4 (2019) 270–276.
[94] Xiaorui Zheng, et al., Highly efficient and ultra-broadband graphene oxide ultrathin lenses with three-dimensional subwavelength focusing, Nat. Commun. 6.1 (2015) 8433.
[95] A.D. Squires, X. Gao, J. Du, Electrically tuneable terahertz metasurface enabled by a graphene/gold bilayer structure, Commun. Mater. 3 (2022) 56.
[96] Hao Chen, et al., Microwave beam reconfiguration based on graphene ribbon, IEEE Trans. Antennas. Propag. 66.11 (2018) 6049–6056.
[97] Hao Chen, et al., Microwave programmable graphene metasurface, ACS Photonics 7.6 (2020) 1425–1435.
[98] Jin Zhang, et al., Dynamic scattering steering with graphene-based coding metamirror, Adv. Opt. Mater. 8.19 (2020) 2000683.
[99] Shibiao Wei, et al., A varifocal graphene metalens for broadband zoom imaging covering the entire visible region, ACS Nano 15.3 (2021) 4769–4776.
[100] Patrick Rufangura, et al., Enhanced absorption with graphene-coated silicon carbide nanowires for mid-infrared nanophotonics, Nanomaterials 11.9 (2021) 2339.
[101] David A. Katzmarek, et al., Direct synthesis of nanopatterned epitaxial graphene on silicon carbide, Nanotechnology 34.40 (2023) 405302.
[102] Rakesh Arul, et al., The mechanism of direct laser writing of graphene features into graphene oxide films involves photoreduction and thermally assisted structural rearrangement, Carbon. N. Y. 99 (2016) 423–431.
[103] Changqing Shen, Fangzhu Qing, Xuesong Li, The etching effect of oxygen during the cooling process of graphene CVD synthesis, Carbon. N. Y. (2024) 119654.
[104] Sehong Park, et al., Electrically focus-tuneable ultrathin lens for high-resolution square subpixels, Light: Sci. Appl. 9.1 (2020) 98.